Materials Science

AIMS Materials Science, 4(3): 800-813.
DOI: 10.3934/matersci.2017.3.800
Received: 24 April 2017
Accepted: 29 June 2017
Published: 03 July 2017

http://www.aimspress.com/journal/Materials

Research article

Synergized mechanistic and solar photocatalysis features of N-TiO_2 functionalised activated carbon

Kah Hon Leong [1,*], Azrina Abd Aziz [2], Yee Li Kang [3], Sheau Wei Goh [3], Kulhar Vijay Singh [4], Lan Ching Sim [1], and Pichiah Saravanan [3,5,*]

[1] Department of Environmental Engineering, Faculty of Engineering and Green Technology, Universiti Tunku Abdul Rahman, Jalan Universiti, Bandar Barat, 31900 Kampar, Perak, Malaysia
[2] Department of Energy and Environment, Faculty of Engineering Technology, Universiti Malaysia Pahang, Lebuhraya TunRazak, 26600 Gambang, Kuantan, Pahang, Malaysia
[3] Environmental Engineering Laboratory, Department of Civil Engineering, Faculty of Engineering, University of Malaya, 50603 Kuala Lumpur, Malaysia
[4] School of Infrastructure, Indian Institute of Technology Bubaneswar, Bubaneswar-751053, India
[5] Environmental Nanotechnology Laboratory, Department of Environmental Science and Engineering, Indian Institute of Technology (ISM) Dhanbad, Dhanbad-826004, Jharkhand, India

* **Correspondence:** Email: pichiahsaravanan@gmail.com; khleong@utar.edu.my.

Abstract: A TiO_2 photocatalysts was successfully functionalised by employing nitrogen (N) as a dopant on activated carbon (AC) support as synergist. Two different types of activated carbon adopting namely *Garcinia mangostana* and palm shell as precursor were chosen as an activated carbon support. Thus the synthesized samples were examined for its physical and chemistry properties through advanced microscopic and spectroscopic techniques. The results revealed the contribution of adsorbent support through the rich surface area while doping of nitrogen contributed for effectively utilizing the incident photons by narrowing the band gap energy. The synergetic adsorption-photocatalytic activity was investigated by adopting batik dye, Remazol Brilliant Blue Dye (RBB) as model pollutant. Thus the N-TiO_2 functionalised activated carbon demonstrated excellent adsorption-photocatalytic activity with 80% removal efficiency in 6 h. The synergism of adsorption-photocatalysis portrayed the alternative for treating recalcitrant RBB a predominant dye found in batik textile industry wastewater.

Keywords: N-TiO_2; activated carbon; functionalization; synergistic; adsorption-photocatalysis

1. Introduction

Remazol Brilliant Blue dye (RBB) is a harmful anthraquinone dye used mainly in the textile industries. The RBB is one of the most common dyes and often used as a primary material in the production of polymeric colorants [1] and classified as recalcitrant and toxic organic pollutants [2]. This injurious dye is capable of damaging the flora and fauna in the aquatic and terrestrial ecosystem [3]. Therefore, an effective treatment is mandatory to eliminate this complex organic pollutant for the benefit of public health and ecological safety. Moreover, their chemical structures make more resistivity towards the existing conventional physicochemical techniques [4–7]. The practiced or available conventional treatment method is only able to transfer the RBB from one phase to another and not to fully transform it into harmless compounds. Thus some alternative technologies are in demand to effectively eliminate RBB from the aqueous solution.

The well-known Advanced Oxidation Processes (AOPs) shows great ability in addressing this issue. Off these the heterogeneous photocatalysis employing TiO_2 as photocatalyst had proven it eco-friendly successfulness in addressing various organic pollutants. This was mainly attributed to its excellent versatile characteristic of possessing high chemical stability, non-toxicity, cost effective, etc. [8–11]. However, the efficiency and practicality of TiO_2 is restricted by its well-known obstacles [12,13,14]. Attempts have been made to overcome its obstacles through doping with non-metal, noble metal, incorporation with organic semiconductor, etc. [15,16,17]. Among the adopted strategy doping with non-metals like C, N, S and F easily incorporates into the lattice of TiO_2 and shifts the band gap energy towards the absorption of visible light [18,19,20]. On the other hand, such doping is one of the ease and economical methods for promoting sustainable approach in the current situations.

Furthermore, functionalising TiO_2 on porous activated carbon (AC) will lead to synergisation and would exhibit greater ability for treating organic compounds. This superior contribution is sustained by its high specific surface area, high degree of surface reactivity and relatively low cost [21–25]. Therefore, activated carbon will be one of the most cost effective supports with proven adsorption capacity for synergizing the adsorption-photocatalytic oxidations process in upsurge the photacatalytic reaction with organic pollutants especially textile dye [26,27,28].

The present work embarks on intensification of N-TiO_2 with AC for synergized performance for treating the aquatic pollutant. The nitrogen doped TiO_2 was successfully synthesized and was functionalised on two different AC derived from *Garcinia Mangostana* shell (GAC) and palm shell (CAC). Off these GAC was prepared in our laboratory and CAC was commercial obtained from the market. Thus fabricated N-TiO_2/AC was characterized and functionalized for the removal of RBB dye under direct sunlight. This present work will be a promising alternative solution for destructing such recalcitrant pollutant through a sustainable approach.

2. Material and Methods

2.1. Materials

CAC of <1 mm, manufactured using commercial palm oil mill waste as precursor was obtained from Bravo Green SdnBhd, Malaysia while the GAC was synthesized in our laboratory [29]. Orthophosphoric acid (H_3PO_4, ≥99% trace metals basis), Sodium bi carbonate ($NaHCO_3$, 99.5–

100.5%), Sodium sulphate (Na_2SO_4, ≥99% trace metals basis), Barium chloride ($BaCl_2$, ≥99% trace metals basis) and Titanium (III) sulphate solution ($Ti_2(SO_4)_3$, ≥99% trace metals basis) were purchased from Sigma Aldrich and used without further purification. Milli-Q water (18.2 MΩ·cm) was used for all the experiments.

2.2. Functionalisation of N-TiO_2 on AC

The details on preparation of AC from *Garcinia Mangostana* shell and N doping are detailed in our earlier reports [29]. The functionalisation of N-TiO_2 onto AC was carried out by adding 1 g of N-TiO_2 and AC each into 1 L of Milli-Q water. The mixture was homogenized through prolonged stirring at room temperature (27 ± 2 °C). Then the product was centrifuged and dried over night at 100 ± 2 °C. The dried product was then carbonized in the furnace at 400 °C for an hour.

2.3. Characterization

Crystallography identifications (XRD) were performed using a Bruker diffractometer (D8) with Cu K_α emission of wavelength (λ) 1.5406 Å. The angular 2θ diffraction was varied between 10 and 80° with the data collection completed at the step size of 0.02° with the step time of 1 s. The crystallite sizes were calculated by using the Debye-Scherrer equation. Field emission scanning electron microscope (FESEM) equipped with energy dispersive X-ray (EDX) silicon drift detector (SDD) (Hitachi SU-8000) was used to investigate the morphology and the inorganic compositions of prepared photocatalysts. Brunauer–Emmett–Teller (BET) surface area, pore volume, and Barret–Joyner–Halenda (BJH) pore size distribution (PSD) based on N adsorption-desorption isotherms were analyzed by QuantachromeAutosorb Automated Gas Sorption System. The degassing of the sample was carried out at 150 °C for 5 h with nitrogen gas. Thermo Nicolet iS10 Fourier Transform Infrared (FTIR) Spectroscope was used to analyze the functional group transmittance between 500 and 4000 cm^{-1}. X-ray photoelectron analysis (XPS) was carried out using Axis Ultra DLD instrument of KRATOS using monochromatic Al-K_α radiation (225 W, 15 mA, 15 kV). The binding energy (BE) of adventitious C ls = 284.9 eV was used as reference. The observed spectrums were indicated by a curve-fitting process, assuming the Gaussian-Lorentzian function. The optical absorption study was evaluated using UV-Vis Spectrophotometer (Shimadzu UV-2600) equipped with $BaSO_4$ diffuse reflectance integrating sphere (DRS) at ambient temperature in the wavelength range between 200 and 800 nm.

2.4. Synergetic Adsorption-photoactivity Evaluation

Synergetic adsorption-photocatalytic study was carried out in a batch reactor of 1 L capacity with a working volume of 250 mL. The reactor adopted a simple glass beaker, under stirred condition using a magnetic stirrer. A dedicated adsorption process was carried out in a dark condition until adsorption equilibrium (1 h) was achieved. This was followed by photocatalysis under direct solar light. All the photocatalytic experiments were carried in a good sunny day under identical conditions. The intensity of sunlight which varied between 80 and 210 $W \cdot m^{-2}$ was measured using LT Lutron LX-101 light meter. The intensified adsorption-photocatalytic experiments were performed with a synergized catalyst of 1 g with 50 mg/L of initial dye concentration. Prior to the experiments the dye solutions was vigorously stirred for uniform dye concentration. The samples were collected at regular time interval, filtered and the supernatant was subsequently analyzed for the residual dye concentration. The concentrations of RBB solution were determined by measuring the absorbance at 596 nm with the UV-Vis spectrophotometer.

3. Results and Discussion

3.1. Structural and Morphology Properties

Figure 1 shows the XRD pattern for N-TiO_2, N-TiO_2/CAC and N-TiO_2/GAC. All the diffraction peaks in Figure 1 showed the complete formation of body-centered tetragonalanatase phase of TiO_2. This was indexed according to JCPDS card No. 21-1272 and the lattice plane was confirmed by diffraction peaks (101), (004), (200), (211), (204), and (301) at 2θ = 25.3, 37.8, 48.0, 55.1, 62.7, 76.0°. No diffraction peaks, either related to rutile or brookite phases were observed in the prepared N-TiO_2 samples. However, a minor primitive rutile phase peak was detected at 27.5° (110) in the composite samples. This was mainly attributed to the heat treatment adopted in the functionalisation step [5]. Further, the functionalisation leads to instability of anatase phase. The presence of amorphous carbon in both the synergized samples proved the formation of the adsorbent as a synergist to the photocatalyst. The average particle sizes of TiO_2 calculated from Debye-Scherrer equation were found to be 33.49 nm for N-TiO_2 and 61.91 nm for both N-TiO_2/CAC and N-TiO_2/GAC.

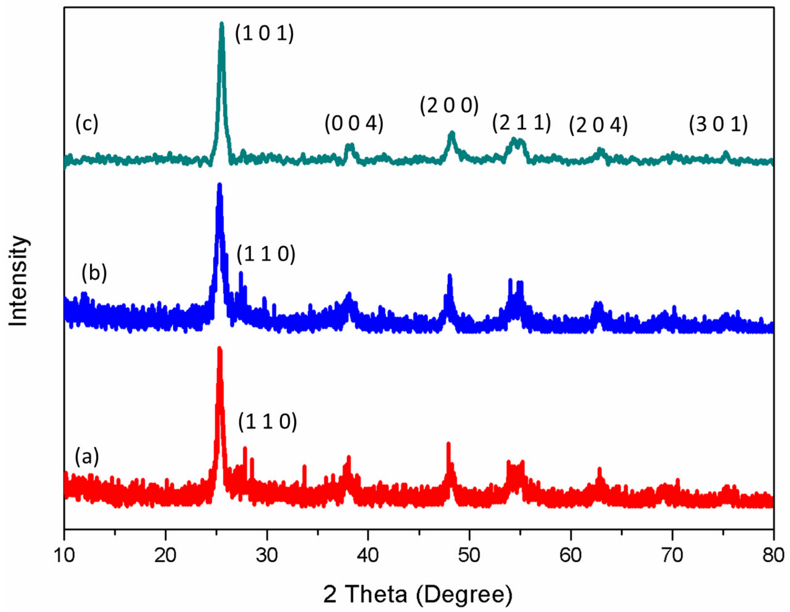

Figure 1. Diffraction pattern of (a) N-TiO_2/GAC, (b) N-TiO_2/CAC and (c) N-TiO_2.

The morphology and texture of the prepared samples were depicted in Figure 2. The spherical morphology with relatively uniform pores was inferred for the N-TiO_2 as shown in Figure 2a and 2b. Meanwhile, the functionalised illustrated a fairly uniform morphology with a minimum number of pores as portrait in Figure 2c and 2d. However, the pore size of the N-TiO_2/CAC is larger and even as compared to N-TiO_2/GAC. The images in Figure 2e and 2f clarify the distributions of the pores derived after the functionalisation of N-TiO_2.

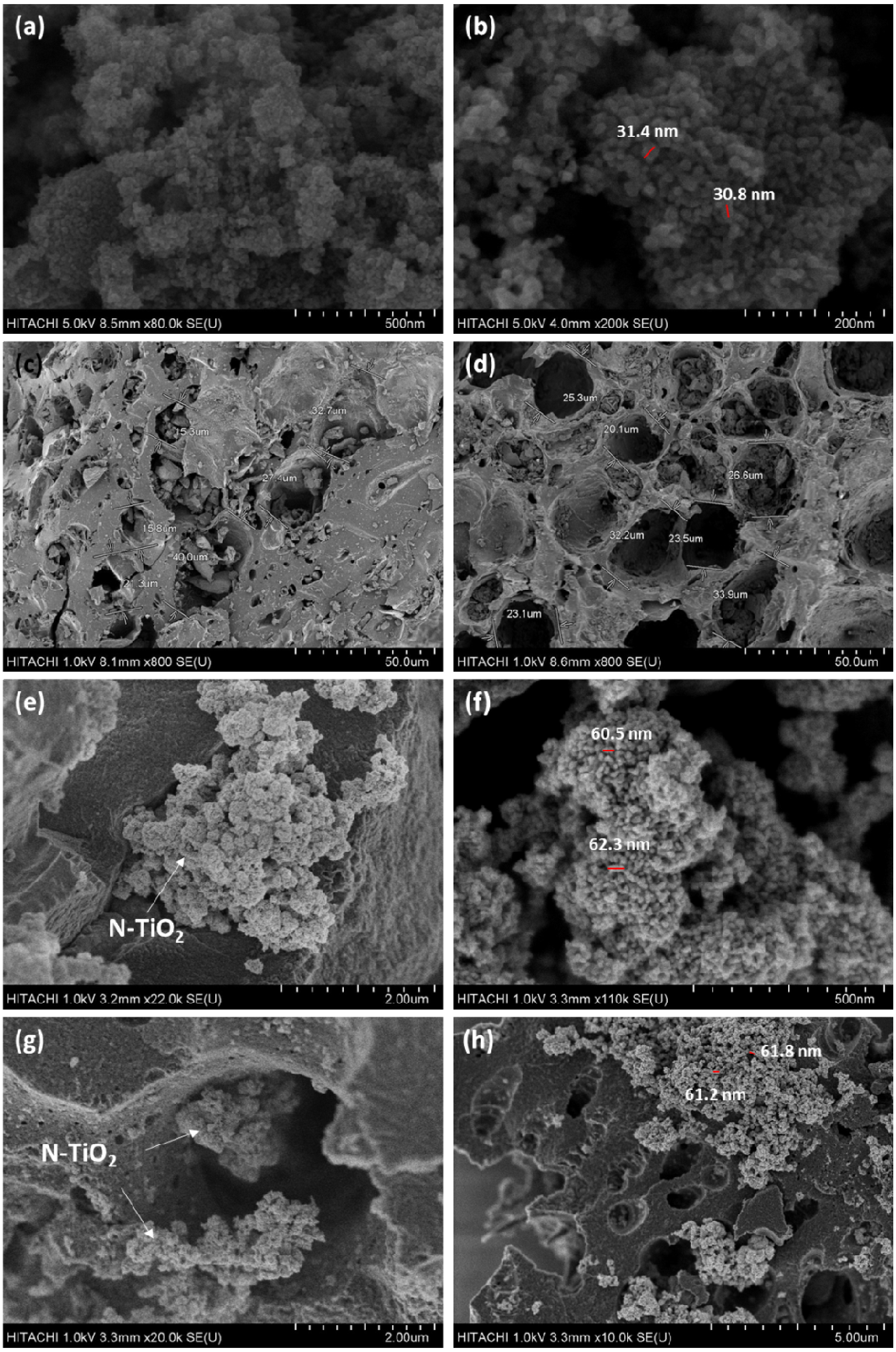

Figure 2. Topography of (a–b) N-TiO_2, (c) GAC, (d) CAC, (e–f) N-TiO_2/GAC, (g–h) N-TiO_2/CAC.

The EDX spectra of the prepared catalysts are illustrated in Figure 3 and the elemental mapping shows that N-TiO_2/GAC contain 48.58 wt% of C, 29.48 wt% of O, 14.89 wt% of Ti, 6.44 wt% of N and 0.61 wt% of P. The trivial occurrence of phosphate was due to the usage of H_3PO_4 acid during the preparation of GAC. Meanwhile, N-TiO_2/CAC comprise of 55.84 wt% of C, 19.43 wt% of O, 19.56 wt% of Ti and 5.17 wt% of N. Both the photocatalyst functionalised samples recorded a highest percentage of carbon that indicates good attachment of N-TiO_2 with AC [30,31].

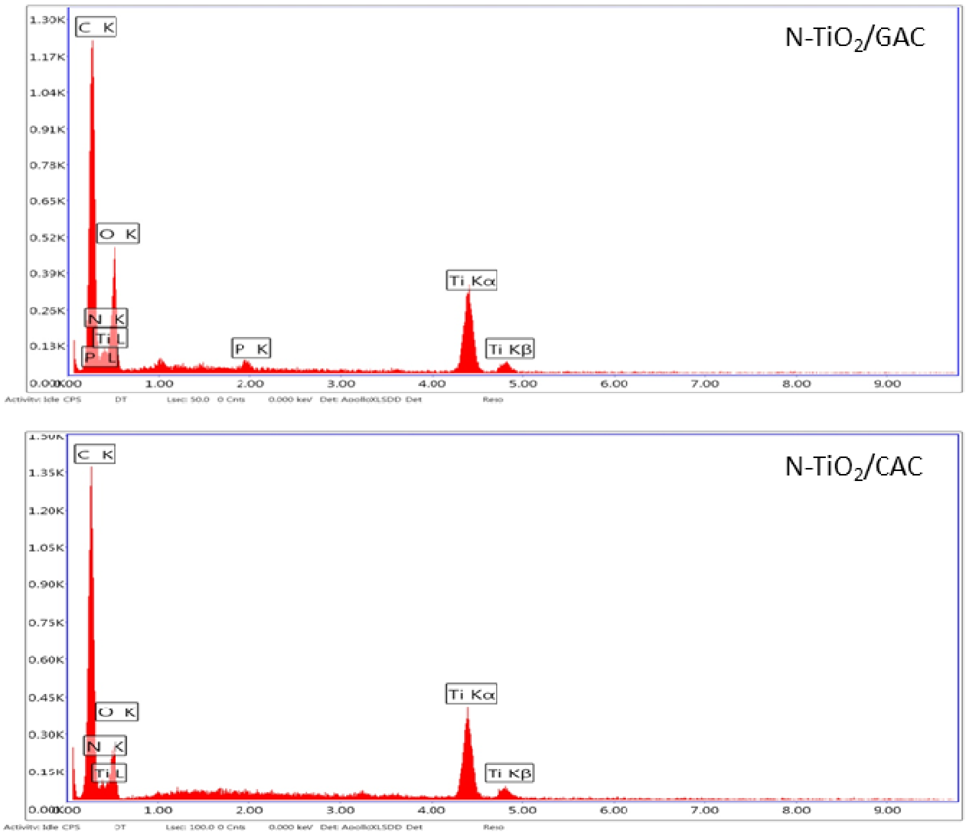

Figure 3. Elemental mapping of functionlised samples.

3.2. Surface Area Analysis

Figure 4 portraits the adsorption-desorption hysteresis and pore size distribution (PSD) of the prepared intensified photocatalysts. Table 1 lists the BET surface area; pore volume and average pore diameter of the samples. From the table, it is observed that the surface area and pore volume of pure GAC is higher than that of pure CAC due to the appropriate synthesis method of GAC. N-TiO_2 exhibited type II hysteresis of BET isotherm with cylindrical pores. The GAC functionalised with photocatalyst showed a type IV classification of BET isotherm, a common type for AC, indicates that dominance of the AC in the surface pores. The functionalised nano sized N-TiO_2 has percolate into the macro and mesopores blocking the micropores resulted in decline of surface area of GAC. This is further clarified through decrease in pore volume of N-TiO_2/GAC [5,32,33,34]. Similarly, the N-TiO_2/CAC showed type IV isotherm, however with lesser N-TiO_2 blocking the micropores as justified in our FESEM images give rise to the higher surface area. This was further substantiated through marginal decrease in the pore volume (0.4357 cm^3/g). Further, the percolation effect and the surface presence of the N-TiO_2 on the AC pores is well observed from the morphological images which contribute to the improved photocatalysis.

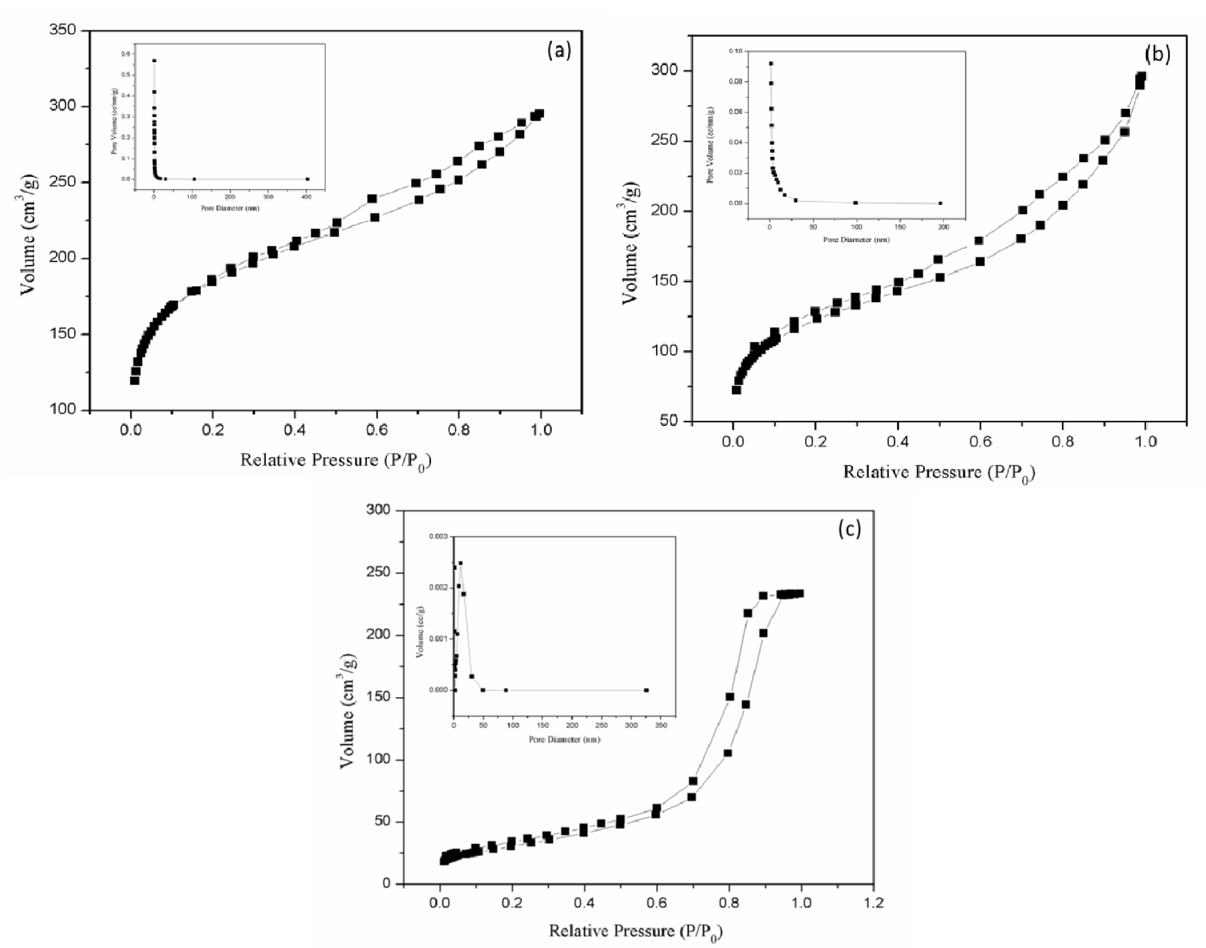

Figure 4. Adsorption-desorption isotherm and BJH pore size distribution curve of (a) N-TiO_2/CAC, (b) N-TiO_2/GAC, (c) N-TiO_2.

Table 1. BET surface area, pore volume and average pore diameter of the AC and prepared photocatalysts.

Samples	BET surface area ($m^2 \cdot g^{-1}$)	Pore volume ($cm^3 \cdot g^{-1}$)	Average pore diameter (nm)
N-TiO_2	106.3	0.3592	13.51
GAC	1218.0	0.7510	2.47
CAC	974.8	0.4480	1.84
N-TiO_2/GAC	343.6	0.3968	4.62
N-TiO_2/CAC	689.0	0.4357	2.53

3.3. FTIR Analysis

Figure 5 explained the functional group transmittance of the prepared photocatalysts. In Figure 5(c), a strong broad distorted peak was inferred in the spectrum between 3300 and 3500 cm^{-1} indicated the presence of hydroxyl groups (O–H) from the acid base character modification of prepare photocatalyst [31]. It also observed in the spectrum that there is a weak intensity of primary amines (N–H) between 3200 and 3500 cm^{-1}. Such amines are contributed by the incomplete removal of HNO_3 [29]. However a stretching vibration of H–O–H bonding of water was recorded for spectrum between 1500 and 1800 cm^{-1}. Figure 5a and 5b showed the ν_{OH} vibration shifted from 3300–3500 cm^{-1} to 3600–4000 cm^{-1}. These vibration shifts was attributed to the incremental positive charge derived from O–H groups, absorbed on the surface of the N-TiO_2 [31]. Furthermore, between 1400–1600 cm^{-1} region shows another strong peak which can be attributed to C=C and C=O skeleton vibration of the aromatic ring. The presence of signals from 2250–2500 cm^{-1} is mainly due to the impurities of N doping. However, the impurity does not tamper either the chemical structure of the composite nor the performance of it [35,36].

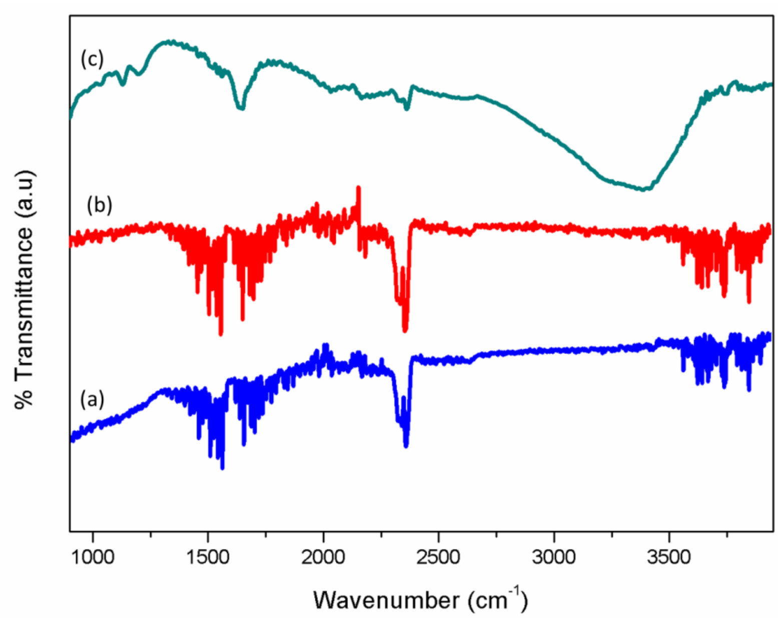

Figure 5. Functional group spectrum of (a) N-TiO_2/CAC, (b) N-TiO_2/GAC and (c) N-TiO_2.

3.4. XPS Analysis

The obtained chemical state spectrums of the prepared photocatalyst are displayed in Figure 6. X-ray spectroscopy was applied to the spectral regions of Ti 2p between binding energy 459.1 and 464.8 eV was indexed to the Ti $2p_{3/2}$ and Ti $2p_{1/2}$ photoelectrons in the Ti^{4+} chemical state respectively [25]. The presence of Ti is considered as an active element for the photocatalytic activity. Meanwhile, two distinguish peaks were detected under C 1s spectra. The peaks at 284.5 eV matches to the C–C bonded species which mainly attributed from the activated carbon. The peak located at 288.8 eV is assigned to the formation of C=O species that are resultant from the substitution of lattice titanium atoms with the formation of Ti–O–C bond structures. The fitted O 1s spectra at 531.6 eV indicated the presence of Ti–OH species. A peak centered at 532.7 eV is assigned to the formation of Ti–O–C bond. The N 1s spectra showed the presence of N–H at 399.2 eV contributed to the anionic doping that supported the visible light enhancement [37].

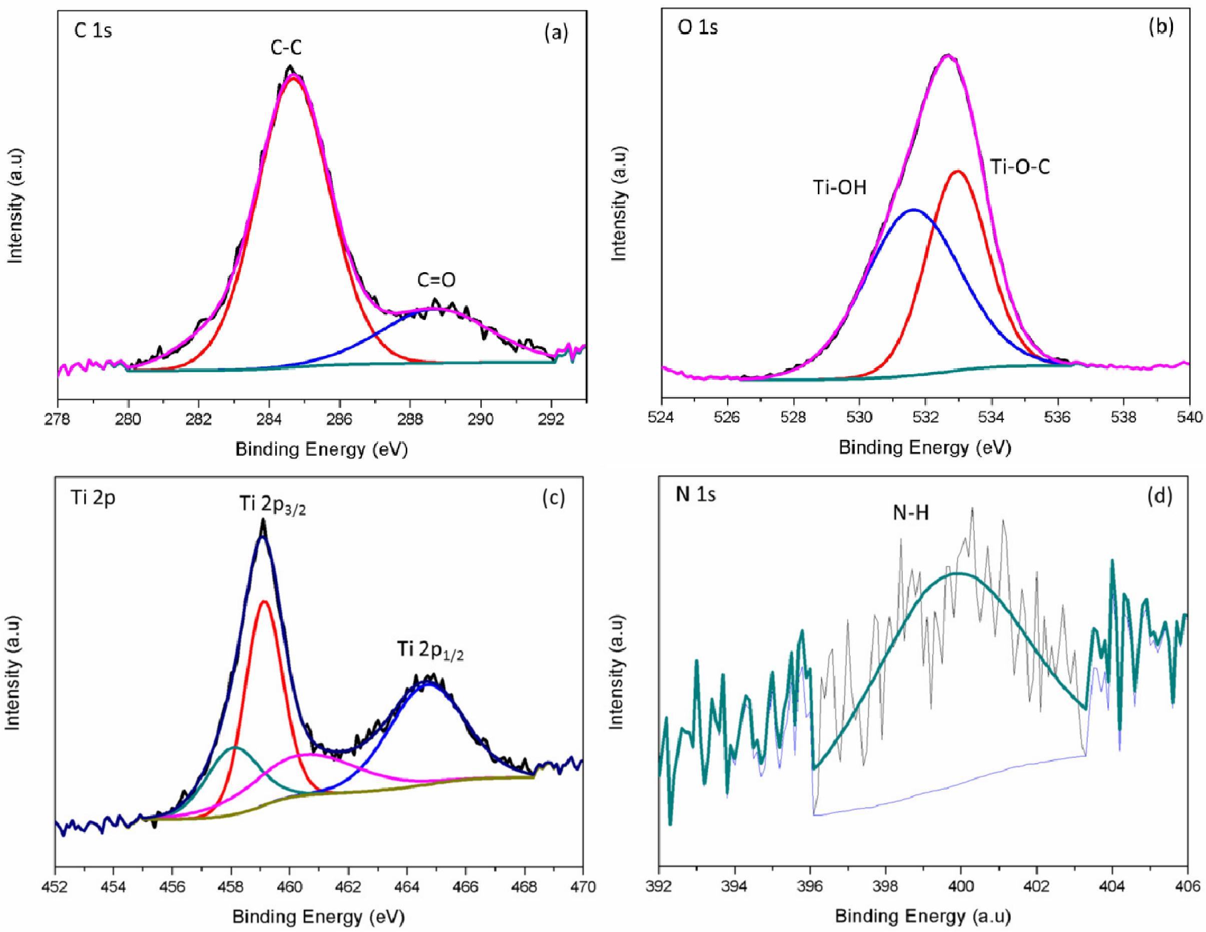

Figure 6. Chemical and electronic state (a) C 1s, (b) O 1s, (c) Ti 2p, and (d) N 1s.

3.5. UV-Vis Absorption Spectra

The UV-visible absorption spectra obtained for the samples were presented in Figure 7. The obtained spectrum illustrates the light response of N-TiO_2 and N-TiO_2 functionalised AC. All the prepared samples exhibited an enhanced absorption in the visible light region along with a notable shift towards longer wavelength. Among them N-TiO_2/AC emerged with a greater adsorption under visible light region and was primarily attributed to the contribution of the carbon support because of synergization due to the black characteristic of AC [30,38]. Moreover, the carbon further contributed to an increase of sacrificial electric charge of oxides in N-TiO_2 [31,39].

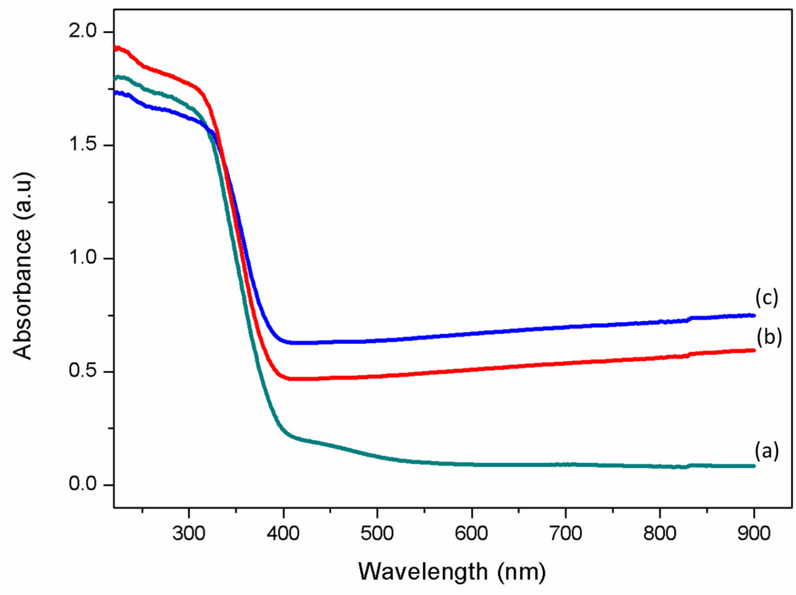

Figure 7. UV-visible absorption profile of (a) N-TiO_2, (b) N-TiO_2/GAC and (c) N-TiO_2/CAC.

3.6. Synergetic Adsorption-photocatalytic Activity

The synergetic adsorption-photocatalytic degradation of RBB Dye with the prepared samples were shown in Figure 8. The N-TiO_2/GAC resulted with a maximum removal efficiency of 80%; while N-TiO_2/CAC resulted with 45% degradation within 6 h of solar light illumination. The non-functionalised showed a poor performance with 30% removal efficiency. A blank experiment was carried out to ensure the photolysis effect. The improved photodegradation performance of N TiO_2 funcationalised samples revealed the homogenous deposition of TiO_2 on to the surface of AC. This facilitated the active electron mobility resulted in generation of active radicals and is clear from the topography obtained from electron microscope.

Under the dark condition, both the N-TiO_2 supported with AC show great adsorption efficiency due to the presence of RBB as RBB^+ form [40]. N-TiO_2/CAC with higher surface area shows better adsorption ability comparing with N-TiO_2/GAC. This rich surface area offering more sites to adsorb RBB resulted in further improving the photocatalytic performance. Additionally, when the sample is exposed to solar irradiation, higher concentration of RBB attached on the photocatalysts surface plays a key role for the acceleration of photochemical reactions between RBB and photocatalysts. It is well known that N doping enables visible light absorption ability of TiO_2 [37]. In addition, the dopant has tendency to exist above the valence band for the exchange of nitrogen (N 2p) [25]. Consequently, the N-TiO_2 illuminated by solar light triggers the electron of valence band to conduction band leaving behind a hole. The excited electrons expected to shift from the N 2p states above the valence band of TiO_2 to the conduction band and get trapped by the surface absorbed O_2. Thus excited electron-hole pairs activate the redox reactions on the surface of the titania, generates active species [25]. These generated species strongly oxidize RBB continuously leading to the formation of harmless CO_2 and H_2O mostly with minor portion of harmless intermediates.

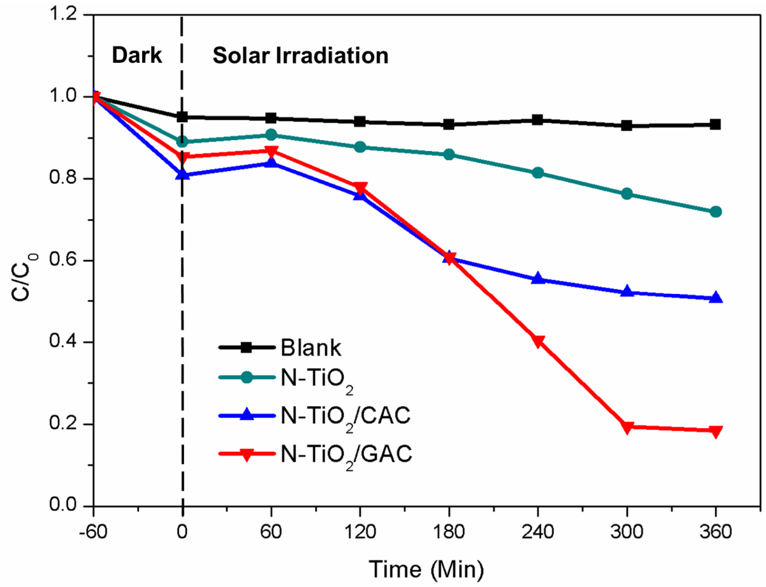

Figure 8. Synergetic adsorption-photocatalytic oxidation of prepared samples.

The obtained promising result was attributed to functionalized N-TiO_2 anatase stability and its robust utilization of photons. Moreover, the AC has proven its ability in contributing for enhancement of photocatalysis reaction through synergistic effect obtained by forming a strong interface between both the AC and N-TiO_2 phase [41]. The AC support also contributed for the enhanced photocatalysis by providing rich surface area that allowed the concentration of RBB dye around the funcationalised titania [42]. This phenomenon well supported the photo-degradation process resulting from the close interface [22]. Furthermore, when the dye was exposed to solar light it undergoes photosensitized oxidation where an electron is excited from the dye and move into the conduction band of TiO_2. As a result, the RBB dyes transformed into cationic dye radicals and undergo further degradation. The interaction of pollutant with photocatalyst driven under the solar irradiation is schematically illustrated in Figure 9.

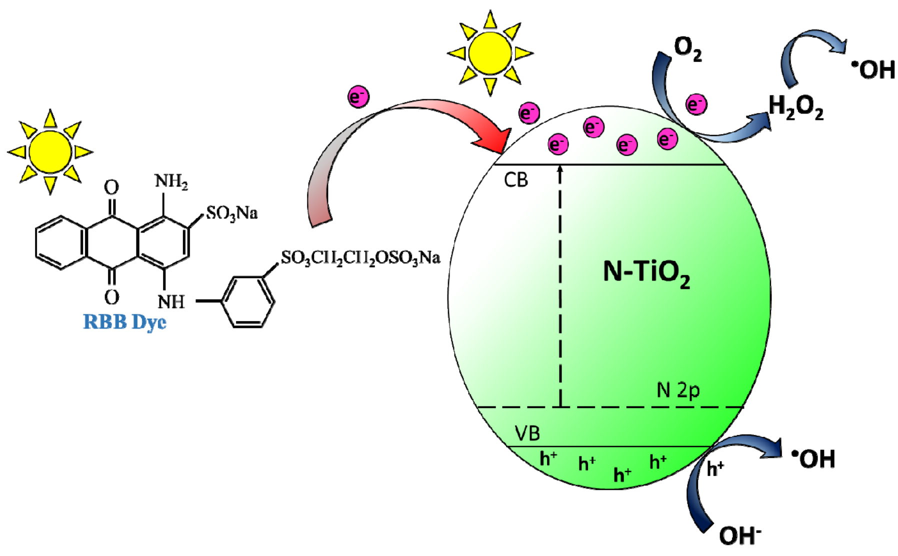

Figure 9. Mechanistic interaction of RBB with N-TiO_2 excited under solar energy.

4. Conclusions

Synergetic N-TiO_2 functionalised AC was successfully synthesized and demonstrated its synergized effect through a photocatalysis reaction driven under solar energy. The attachment of N-TiO_2 had improved absorbance towards the visible light region ensuring the maximum and active utilization of solar spectrum. The carbon derived from the AC also acted as a key contributor for enhancement of photocatalytic activity by shrinking the gap energy. The inherent synergisation well contributed for the completed removal RBB dye by utilizing solar energy. The synergetic effect also contributed for adsorption that further enhanced the removal of dye. Thus the present study established the vibrant applicability of the developed functionalised AC in promoting a sustainable environmental remediation.

Acknowledgements

This research work was supported by University of Malaya Research Grant (UMRG) (RG167/12SUS) and High Impact Research (HIR) Grant (UM.C/625/1/HIR/053/2).

Conflict of Interest

The authors declare that there is no conflict of interest regarding the publication of this manuscript.

References

1. Ada K, Ergene A, Tan S, et al. (2009) Adsorption of remazol brilliant blue R using ZnO fine powder: equilibrium, kinetic and thermodynamic modeling studies. *J Hazard Mater* 165: 637–644.
2. Mechichi T, Mhiri N, Sayadi S (2006) Remazol brilliant blue R decolourization by the laccase from *Trametestrogii*. *Chemosphere* 64: 998–1005.
3. Ahmad AL, Harris WA, Ooi BS (2002) Removal of dye from wastewater of textile industry using membrane technology. *Jurnal Teknologi* 36: 31–44.
4. Bhatnagar A, Jain A (2005) A comparative adsorption study with different industrial wastes as adsorbents for the removal of cationic dyes from water. *J Colloid Interf Sci* 281: 49–55.
5. Foo K, Hameed B (2010) Decontamination of textile wastewater via TiO_2/activated carbon composite materials. *Adv Colloid Interfac* 159: 130–143.
6. Chu SY, Xiao JB, Tian GM, et al. (2014) Preparation and characterization of activated carbon from aquatic macrophyte debris and its ability to adsorb anthraquinone dyes. *J Ind Eng Chem* 20: 3461–3466.
7. Mahmoodi NM, Sadeghi U, Maleki A, et al. (2014) Synthesis of cationic polymeric adsorbent and dye removal isotherm, kinetic and thermodynamic. *J Ind Eng Chem* 20: 2745–2753.
8. Sharon M, Modi F, Sharon M (2016) Titania based nanocomposites as a photocatalyst: A review. *AIMS Mater Sci* 3: 1236–1254.
9. Collazzo GC, Foletto EL, Jahn SL, et al. (2012) Degradation of direct black 38 dye under visible light and sunlight irradiation by N-doped anatase TiO_2 as photocatalyst. *J Environ Manage* 98: 107–111.

10. Velmurugan R, Krishnakumar B, Subash B, et al. (2013) Preparation and characterization of carbon nanoparticles loaded TiO_2 and its catalytic activity driven by natural sunlight. *Sol Energ Mat Sol C* 108: 205–212.
11. Asiltürk M, ŞenerŞ (2012) TiO_2-activated carbon photocatalysts: Preparation, characterization and photocatalytic activities. *Chem Eng J* 180: 354–363.
12. Baek MH, Jung WC, Yoon JW, et al. (2013) Preparation, characterization and photocatalytic activity evaluation of micro and mesoporous TiO_2/spherical activated carbon. *J Ind Eng Chem* 19: 469–477.
13. Lee SY, Park SJ (2013) TiO_2 photocatalyst for water treatment applications. *J Ind Eng Chem* 19: 1761–1769.
14. Sun JH, Wang YK, Sun RX, et al. (2009) Photodegradation of azo dye Congo Red from aqueous solution by the WO_3-TiO_2/activated carbon (AC) photocatalyst under the UV irradiation. *Mater Chem Phys* 115: 303–308.
15. Leong KH, Gan BL, Ibrahim S, et al. (2014) Synthesis of surface plasmon resonance (SPR) triggered Ag/TiO_2 photocatalyst for degradation of endocrine disturbing compounds. *Appl Surf Sci* 319: 128–135.
16. Eslami A, Amini MM, Yazdanbakhsh AR, et al. (2016) N, S co-doped TiO_2 nanoparticles and nanosheets in simulated solar light for photocatalytic degradation of non-steroidal anti-inflammatory drugs in water: a comparative study. *J Chem Technol Biot* 91: 2693–2704.
17. Adhikari SP, Awasthi GP, Kim HJ, et al. (2016) Electrospinning directly synthesized porous TiO_2 nanofibers modified by graphitic carbon nitride sheets for enhanced photocatalytic degradation activity under solar light irradiation. *Langmuir* 32: 6163–6175.
18. Fan JM, Zhao ZH, Liu WH, et al. (2016) Solvothermal synthesis of different phase N-TiO_2 and their kinetics, isotherm and thermodynamic studies on the adsorption of methyl orange. *J Colloid Interf Sci* 470: 229–236.
19. Fagan R, McCormack DE, Hinder S, et al. (2016) Improved high temperature stability of anatase TiO_2 Photocatalysts by N, F, P co-doping. *Mater Des* 96: 44–53.
20. Lei XF, Xue XX, Yang H, et al. (2015) Visible light-responded C, N and S co-doped anatase TiO_2 for photocatalytic reduction of Cr(VI). *J Alloy Compd* 646: 541–549.
21. Wang X, Hu Z, Chen Y, et al. (2009) A novel approach towards high-performance composite photocatalyst of TiO_2 deposited on activated carbon. *Appl Surf Sci* 255: 3953–3958.
22. Ragupathy S, Raghu K, Prabu P (2015) Synthesis and characterization of TiO_2 loaded cashew nut shell activated carbon and photocatalytic activity on BG and MB dyes under sunlight radiation. *Spectrochim Acta A* 138: 314–320.
23. Alalm MG, Tawfik A, Ookawara S (2016) Solar photocatalytic degradation of phenol by TiO_2/AC prepared by temperature impregnation method. *Desalin Water Treat* 57: 835–844.
24. Liu C, Li YJ, Xu P, et al. (2015) Controlled synthesis of ordered mesoporous TiO_2 supported on activated carbon and pore-pore synergistic photocatalytic performance. *Mater Chem Phys* 149: 69–76.
25. Liu D, Wu Z, Tian F, et al. (2016) Synthesis of N and La co-doped TiO_2/AC photocatalyst by microwave irradiation for the photocatalytic degradation of naphthalene. *J Alloy Compd* 676: 489–498.
26. Berrios M, Martín MA, Martín A (2012) Treatment of pollutants in wastewater: Adsorption of methylene blue onto olive-based activated carbon. *J Ind Eng Chem* 18: 780–784.

27. Wang X, Hu Z, Chen Y, et al. (2009) A novel approach towards high-performance composite photocatalyst of TiO_2 deposited on activated carbon. *Appl Surf Sci* 255: 3953–3958.
28. Gu L, Chen Z, Sun C, et al. (2010) Photocatalytic degradation of 2,4-dichlorophenol using granular activated carbon supported TiO_2. *Desalination* 263: 107–112.
29. Aziz AA, Yong KS, Ibrahim S, et al. (2012) Enhanced magnetic separation and photocatalytic activity of nitrogen doped titania photocatalyst supported on strontium ferrite. *J Hazard Mater* 199: 143–150.
30. Arana J, Dona-Rodrıguez J, Tello Rendón E, et al. (2003) TiO_2 activation by using activated carbon as a support: Part 1. Surface characterisation and decantability study. *Appl Catal B-Environ* 44: 161–172.
31. Ravichandran L, Selvam K, Swaminathan M (2010) Highly efficient activated carbon loaded TiO_2 for photodefluoridation of pentafluorobenzoic acid. *J Mol Catal A-Chem* 317: 89–96.
32. Lee DK, Kim SC, Cho IC, et al. (2004) Photocatalytic oxidation of microcystin-LR in a fluidized bed reactor having TiO_2-coated activated carbon. *Sep Purif Technol* 34: 59–66.
33. Subramani AK, Byrappa K, Kumaraswamy GN, et al. (2007) Hydrothermal preparation and characterization of TiO_2: AC composites. *Mater Lett* 61: 4828–4831.
34. Ao Y, Xu J, Fu D, et al. (2008) Low temperature preparation of anatase TiO_2-coated activated carbon. *Colloid Surface A* 312: 125–130.
35. Han C, Wang Y, Lei Y, et al. (2015) *In situ* synthesis of graphitic-C_3N_4 nanosheet hybridized N-doped TiO_2 nanofibers for efficient photocatalytic H_2 production and degradation. *Nano Res* 8: 1199–1209.
36. Abdullah AM, Al-Thani NJ, Tawbi K, et al. (2016) Carbon/nitrogen-doped TiO_2: New synthesis route, characterization and application for phenol degradation. *Arab J Chem* 2: 229–237.
37. Fu X, Yang H, Sun H, et al. (2016) The multiple roles of ethylenediamine modification at TiO_2/activated carbon in determining adsorption and visible-light-driven photoreduction of aqueous Cr(VI). *J Alloy Compd* 662: 165–172.
38. Li Y, Zhou X, Chen W, et al. (2012) Photodecolorization of Rhodamine B on tungsten-doped TiO_2/activated carbon under visible-light irradiation. *J Hazard Mater* 227: 25–33.
39. Bedja I, Hotchandani S, Kamat PV (1993) Photoelectrochemistry of quantized tungsten trioxide colloids: electron storage, electrochromic, and photoelectrochromic effects. *J Phys Chem* 97: 11064–11070.
40. Kannan N, Sundaram MM (2001) Kinetics and mechanism of removal of methylene blue by adsorption on various carbons—a comparative study. *Dyes Pigments* 51: 25–40.
41. Zhou J, Li F, Du C, et al. (2016) Photodegradation performance and recyclability of a porous nitrogen and carbon co-doped TiO_2/activated carbon composite prepared by an extremely fast one-step microwave method. *RSC Adv* 6: 84457–84463.
42. Le HA, Linh LT, Chin S, et al. (2012) Photocatalytic degradation of methylene blue by a combination of TiO_2-anatase and coconut shell activated carbon. *Powder Technol* 225: 167–175.